RESEARCH ARTICLE

Subsonic jet pressure fluctuation characterization by tomographic laser interferometry

**Milena Martarelli · Paolo Castellini ·
Enrico Primo Tomasini**

Abstract This paper describes the application of a non-conventional experimental technique based on optical interferometry for the characterization of aeroacoustic sources. The specific test case studied is a turbulent subsonic jet. Traditional experimental methods exploited for the measurement of aerodynamic velocity fields are laser Doppler anemometer and particle image velocimetry which have an important drawback due to the fact that they can measure only if the flow is seeded with tracer particles. The technique proposed, by exploiting a laser Doppler interferometer and a tomographic algorithm for 3D field reconstruction, overcomes the problem of the flow seeding since it allows directly measuring the flow pressure fluctuation due to the flow turbulence. A laser Doppler interferometer indeed is sensitive to the density oscillation within the medium traversed by the laser beam even though it integrates the density oscillation along the entire path traveled by the laser. Consequently, the 3D distribution of the flow density fluctuation can be recovered only by exploiting a tomographic reconstruction algorithm applied to several projections. Finally, the flow pressure fluctuation can be inferred from the flow density measured, which comprehends both the aerodynamic pressure related to the turbulence and the sound pressure due to the propagation of the acoustic waves into the far field. In relation to the test case studied in this paper, e.g., the turbulent subsonic jet, the method allows a complete aeroacoustic characterization of the flow field since it measures both the aerodynamic "cause" of the noise, such as the vortex shedding, and the acoustic "effect" of it, i.e., the sound propagation in the 3D space. The performances and the uncertainty have been evaluated and discussed, and the technique has been experimentally validated.

1 Introduction

Environmental noise is increasingly becoming a community concern being one of the most common pollutants, and a worldwide rule is to promote noise mitigation measures. One of the most annoying noise sources polluting the environment is related to turbulent jets. Jet noise is generated by the fluid-dynamic process related to the turbulent mixing of vortex structures with the surrounding steady air. The aeroacoustic characterization of turbulent jets is conventionally performed starting from the measurement of the fluid-dynamic phenomena generating the jet noise, and therefore, the effect, i.e., the sound field, is achieved by applying the Lighthill analogy (Fischer and Sauvage 2008). The cause of the noise, being of aerodynamic nature, is typically estimated via experimental techniques measuring the flow velocity and turbulence such as constant temperature anemometer (CTA), laser Doppler anemometer (LDA), and particle image velocimetry (PIV). Both the last two methods have the advantage of being noninvasive, but the most employed for jet characterization is PIV (Schram et al. 2002; Violato and Scarano 2011). However, this technique has a main drawback due to the fact that it requires seeding the flow since it measures the velocity of the tracer particles that scatter the light diffused by a laser source toward a CMOS camera. The basic assumption of this experimental

M. Martarelli
Faculty of Engineering, Università degli Studi eCampus,
Novedrate, CO, Italy
e-mail: milena.martarelli@uniecampus.it

P. Castellini (✉) · E. P. Tomasini
DIISM, Università Politecnica delle Marche, Via Brecce
Bianche, 60131 Ancona, Italy
e-mail: p.castellini@univpm.it

technique is therefore that the seeding particle moves with the same speed of the flow and this is not always a trivial task. The inertia of the tracer particles will limit the high-frequency response of the technique. Besides, hardware performances, specifically CMOS cameras and pulsed lasers, will restrict the PIV application to quite low frequency ranges, mainly if a significant spatial resolution is required. The LDA technique has also two drawbacks: It always requires seeding the flow and it samples data at irregular sample frequency, and thus, a significant data post-processing is required. The jet noise can be directly measured by applying acoustic techniques that identify the effect of the fluid-dynamic phenomena. The recent advances on phased array techniques, i.e., beamforming (Dougherty and Podboy 2009), for measuring the spatial distribution of acoustic fields, allowed us to measure the noise generated by air jets and to have a sort of its acoustic image. However, beamforming techniques have several limits:

- The measurement input is the sound field, e.g., the effect of the fluid-dynamic phenomena and not its direct cause;
- The spatial resolution is high only at the high frequency range, and therefore, the method cannot apply for identifying noise sources at the low–medium frequency range;
- The technique is sensitive to errors, since an error of 1 % on the aerodynamic pressure field yields an error of 100 % on the acoustic field, and its uncertainty is relatively high (Castellini and Martarelli 2008) for jet applications.

In the recent years, several attempts have been done to improve the experimental procedures aiming at performing the aeroacoustic characterization of turbulent jets. Most of the methods have been focused on the identification of "cause–effects" relationships by combining fluid-dynamic inflow measurements and acoustic far-field measurements. A nonconventional experimental technique that allows us to measure both the fluid-dynamic phenomenon and the sound propagation is represented by the laser Doppler interferometry, an instrument that used to be applied for flow visualization, for example, by Schlieren (Kleine et al. 2006) and Vanherzeele et al. (2007). That technique is sensitive to the variation of the refraction index of the light within the optical path of the laser beam caused by density fluctuations occurring in turbulent flows. The actual quantity measured by the interferometer is the line integral of the density fluctuation over the laser beam optical path. That holding, reconstruction algorithms should be used to calculate local density variation distribution. The use of interferometric techniques for the visualization of flow fields was described by Zipser and Franke (2002) and Mayrhofer and Woisetschläger (2001), but only 2D or rotationally symmetric

distributions were treated, to which inverse Abel transform was applied. An interesting application was shown in Woisetschläger et al. (2003) where a 2D turbine wake flow was investigated and compared to the phase-resolved PIV results. However, it should be pointed out that the interferometric technique and PIV measure different quantities: the density/pressure fluctuation, the first, and the flow velocity, the second one. Laser Doppler interferometer measurements were successfully applied to map density fluctuations in flames by Woisetschläger et al. in Köberl et al. (2010) and Giuliani et al. (2010). A very interesting example of the application of such technique was shown by Tatar et al. (2007) where the laser Doppler interferometer was exploited for the reconstruction of the acoustic field produced by an array of ultrasound probes. When 3D spatial distribution has to be tackled and the axial-symmetry hypothesis does not hold, tomography-based algorithms could be applied to signals acquired from multidirectional observations of the flow field. In Castellini and Martarelli (2006), a method for post-processing the data acquired by the interferometer in order to obtain quantitative evaluation of pressure fluctuations was presented. The technique was named tomographic laser interferometry (TLI). An important advantage of that technique is that the acoustic pressure can be easily achieved once the flow density fluctuation is known, and thus, TLI allows us to derive the effect (e.g., the sound radiation) directly from the cause (e.g., the density fluctuation due to the turbulent occurrences).

In this paper, the authors propose the application of TLI to the aeroacoustic characterization of a subsonic jet. Both the fluid-dynamic turbulences and the sound propagation in the far field will be achieved by following a procedure summarized in several steps:

- First, the variation of the refraction index of the light integrated over the laser beam optical path is measured by means of the laser Doppler interferometer on a high-density grid of points and from different directions of view;
- Then, the volumetric distribution of the refraction index fluctuation is calculated by applying a tomographic reconstruction algorithm;
- Finally, the flow density fluctuation and the resulting sound pressure are achieved at each voxel of the measurement volume, each one considered as a monopole sound source.

2 Measurement procedure theoretical basis

2.1 Flow density fluctuation estimation

If the laser beam of a laser Doppler interferometer travels across a turbulent flow, the density fluctuation about the

ambient density at standard conditions, ρ_0, produced by the turbulence will induce a variation of the optical path traveled by the beam. In this work, the interferometer employed was a commercial laser Doppler vibrometer (LDV), based on the Mach–Zehnder architecture. The LDV gives, as output, the Doppler frequency shift (Δf) proportional to the variation of the optical path (dz/dt) sensed by the laser beam when pointed toward a moving surface. Since the conventional signal measured by LDV is a vibration velocity, for simplicity in this paper the signal measured will be called pseudo-velocity, $v = dz/dt$, which is related to the Doppler frequency shift following Eq. (1):

$$\Delta f = 2 \frac{v}{\lambda_{st}} \tag{1}$$

This pseudo-velocity is referred to the laser wavelength measured at standard conditions, λ_{st}, that is not exact because, in the case when the laser light goes across a turbulent flow, the light wavelength changes with the density fluctuation and the actual laser wavelength (λ) must be considered. Therefore, the true measurement output is the so-called measured pseudo-velocity, v_{meas}:

$$v_{meas}(x, y, t) = v \frac{\lambda}{\lambda_{st}} = \frac{dz}{dt} \frac{\lambda}{\lambda_{st}} = \left(Z \frac{dn}{dt} + n \frac{dZ}{dt} \right) \frac{\lambda}{\lambda_{st}} \tag{2}$$

In Eq. (2) the optical path, z, is a function of two components:

- the geometrical path, Z, whose fluctuation is due to the displacement of the surface where the laser beam impinges. This is the measurement principle of common laser Doppler vibrometers,
- the refraction index, $n(x, y, t)$, which undergoes to spatial and temporal variations produced by the jet turbulence within the measurement volume, the light blue region, shown in Fig. 1.

When moving objects are measured in steady air, the refraction index variation is null and only the second term appears in Eq. (2), i.e., the interferometer input is the displacement of the object surface. This happens in the
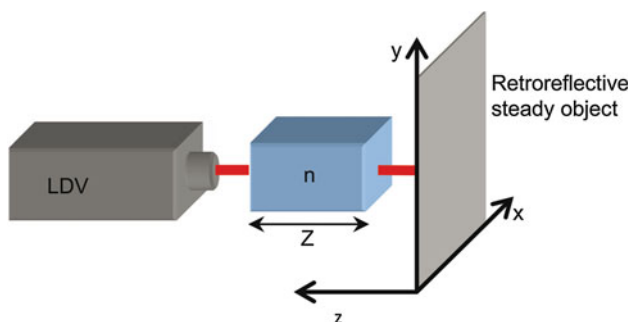

Fig. 1 Mach–Zehnder interferometer configuration

conventional use of LDV. On the other hand, if the laser beam crosses a turbulent region and impinges on a target kept steady, the only variable is the refraction index which fluctuates inside the measuring volume. Being $\lambda n = \lambda_{st} \, n_{st}$ (Edlén 1966) where n_{st} is the index of refraction at standard conditions, Eq. (2) becomes:

$$v_{meas}(x, y, t) = Z \frac{n_{st}}{n(x, y, t)} \frac{dn(x, y, t)}{dt} \tag{3}$$

In this equation the dependence of the refraction index to the z-direction is not considered because the information carried by the laser beam is the integral of n along its optical path. The pseudo-velocity measured by the laser Doppler interferometer v_{meas} can be used to estimate the reflection index variation within the jet turbulent region related to the air density fluctuation (ρ). Conventionally, as in Schlieren-based interferometry (Merzkirch 1974), the relation between n and ρ is given by the Gladstone–Dale relation, developed for fluidic mixtures of several pure compounds. This relation is generally satisfactory. In this paper, instead, a more accurate model linking n and ρ has been used, i.e., the Lorentz–Lorenz equation (Lorentz 1880; Lorenz 1880), the increase in computational effort related to this formulation with respect to the Gladstone–Dale one being quite negligible:

$$\rho(x, y, t) = \frac{W}{A} \frac{n^2(x, y, t) - 1}{n^2(x, y, t) + 2} \tag{4}$$

W being the air molecular weight, i.e., 0.02896 kg/mol, and A the air molar refractivity, i.e., 4.7×10^{-6} m^3/mol (Born and Wolf 1959). Calling $K = \frac{A}{W}$ the index of refraction can be expressed as:

$$n(x, y, t) = \sqrt{\frac{2K\rho(x, y, t) + 1}{1 - K\rho(x, y, t)}} \tag{5}$$

and inserting Eq. (5) in Eq. (3), the vibrometer output pseudo-velocity can be written as follows:

$$v_{meas}(x, y, t) = K \frac{n_{st}}{n(x, y, t)} \frac{1}{2n(x, y, t)} \frac{3K}{[1 - K\rho(x, y, t)]^2} \frac{d\rho(x, y, t)}{dt} \tag{6}$$

This first-order ordinary differential equation can be integrated between two time instants:

- $t_1 = 0$ where the jet is off and $\rho_1 = \rho_0$ (the undisturbed air density), but in practice, the initial air density has been taken equal to zero because the aim of this measurement is to determine density oscillations about the air density at rest (the DC component),
- $t_2 = t$ where $\rho_2 = \rho$,

  thus yielding:

$$\int_0^t v_{\text{meas}}(x,y,t)\,\mathrm{d}t = \frac{3ZK}{2n_{\text{st}}} \int_0^\rho \frac{1}{[1-K\rho(x,y,t)][1+2K\rho(x,y,t)]}\,\mathrm{d}\rho \tag{7}$$

whose integral is the so-called pseudo-displacement, s_{meas}. Thus, the air density oscillation can be recovered from the pseudo-displacement s_{meas} and the known constants K, Z (the measurement volume transversal dimension along the laser line-of-sight), and $n_{\text{st}} = 1.0003$:

$$\rho(x,y,t) = \frac{1}{K} \frac{e^{\frac{2n_{\text{st}}}{Z}s_{\text{meas}}(x,y,t)}}{2 + e^{\frac{2n_{\text{st}}}{Z}s_{\text{meas}}(x,y,t)}} \tag{8}$$

In order to separate the effects occurring at different frequencies, the algorithms presented in this paper are working in frequency domain. Equation (8) becomes thus:

$$\rho(x,y,f) = \frac{1}{K} \frac{e^{\frac{2n_{\text{st}}}{Z}\frac{v_{\text{meas}}(x,y,f)}{2\pi f}}}{2 + e^{\frac{2n_{\text{st}}}{Z}\frac{v_{\text{meas}}(x,y,f)}{2\pi f}}} \tag{9}$$

where f is the frequency in Hz and the pseudo-displacement s_{meas} has been replaced by the pseudo-velocity directly measured by the interferometer.

2.2 Sound pressure calculation

The air density fluctuation will generate a pressure variation consisting on the superimposition of the sound field produced by the vortex occurrences in the near field and the acoustic wave's propagation in the far field. Since the physical mechanism of the pressure fluctuation in a gas is a molecular motion phenomenon (Lorentz 1880; Anderson 1991), the relationship between pressure and density comes from the combination of the perfect gas state equation and the speed of sound in a isentropic flow, c_∞:

$$p(x,y,f) = c_\infty^2 \rho(x,y,f) \tag{10}$$

It can be objected that density and, thus, refraction index fluctuations can be caused by temperature oscillations as well. However, the temperature contribution can be considered less significant with respect to that of pressure (Castellini and Martarelli 2006).

2.3 Tomographic reconstruction of the 3D sound pressure

The output of the previous calculation is the complex pressure $p(x, y, f)$ given in frequency domain. It represents the pressure fluctuation along the optical path of the laser beam (z-direction in Fig. 2), which comes across the measurement volume where the air pressure oscillation causes the variation of the refractive index and therefore
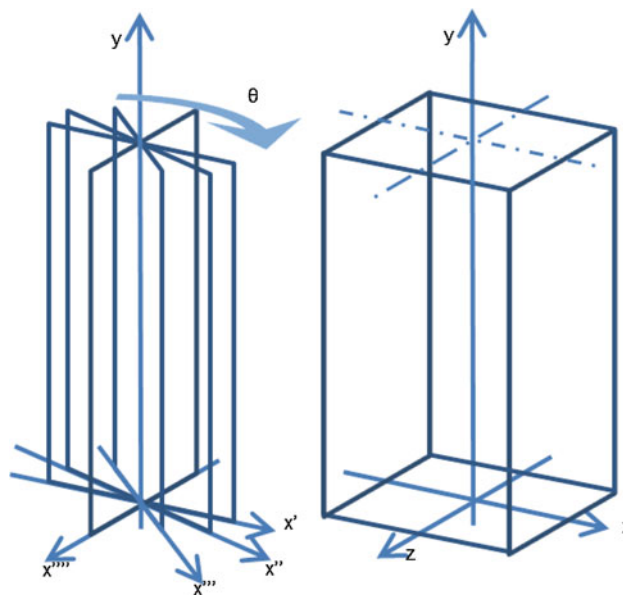

Fig. 2 Reference system scheme before and after the tomography algorithm application

of the air density. The pressure datum must be further transformed on the basis of CT principles, in order to reconstruct the 3D acoustic pressure field. If a sufficient number of projections at different angles of view (θ in Fig. 2a), i.e., a certain number of plane grids, are acquired, the 3D density distribution can be reconstructed, as addressed and discussed by Radon (1917). The theoretical approach of the Radon problem is out of the scope of this paper which, in fact, will only treat its practical implementation. For each projection or angle of view θ_i the sound pressure fluctuation has been measured over a high spatial density point grid. By applying the inverse Radon transform to the set of projections acquired (see Fig. 2a), the Cartesian 3D pressure field can be reconstructed, as in Fig. 2b. The air pressure fluctuation calculated from the interferometric data in the frequency domain can be represented as a complex 4D polar matrix, whose dimensions are the x- and y-coordinates (see Fig. 1) defining the measurement point grid position, the angles of view (θ), and the frequency f. The pressure oscillation measured at each point and for every angle θ corresponds to its integration over the line-of-sight of the laser beam within the measuring volume. By applying the tomography algorithm to that matrix (in practice to its real and imaginary components), the local pressure variation can be recovered on an arbitrary 3D volume, consisting in points called "voxels." The output of the CT process is, therefore, a 4D Cartesian matrix, whose dimensions are the x-, y-, and z-coordinates (see sketch in Fig. 2) and the frequency f.

2.4 TLI application to aeroacoustics

TLI represents an alternative to the experimental techniques for the characterization of aeroacoustic sources. It characterizes the phenomena from a different point of view, with respect to that frequently performed in literature starting from velocity field measurements. The very large experience and tradition in PIV characterization of fluid dynamic triggered the development of velocity studies devoted to the assessment of acoustic data from velocity fields. If coupled to specific acoustic models, the aerodynamic noise generated by the velocity field can be calculated and therefore the far-field acoustic emission estimated, as done in hybrid computational approaches. One of the most well-known aeroacoustic models is based on the Lighthill equation, which comes from a rearrangement of the Navier–Stokes equations, thus allowing us to obtain an inhomogeneous wave equation representing the analogy between acoustics and fluid mechanics. The so-called Lighthill analogy defines how sound generated aerodynamically, i.e., the aerodynamic noise, might be represented through the governing equations of a compressible fluid and links the acoustics to the measured fluid-dynamic velocity and turbulence. In the approach proposed, the analysis is performed directly in terms of density fluctuation. Being the density strictly related to the pressure fluctuation, such technique makes it possible to directly measure the flow-induced/generated noise. The theory behind it consists simply in:

- the law governing the gas optical behavior in terms of its refraction index related to its density by means of the Lorentz–Lorenz equation ref rho3,
- the ideal gas law allowing us to link the air density fluctuation to the aeroacoustic pressure ref.

In addition, the acoustic pressure measured can be used to calculate the far-field sound pressure using the propagation laws considering each voxel as a spherical source or, in the case of vortex shedding, considering each eddy as a quadrupole source. This allows a complementary study, with some potential advantages related to the complexity of aeroacoustics theory due to its multiphysics character. An example of potential exploitation of the technique proposed is that aeroacoustic analogies (Lighthill among others) are frequently based on some assumptions. For instance, the effects of viscosity on the fluid are neglected since it is conventionally accepted that they does not influence the noise generation mechanism. Instead, when measuring directly the flow density oscillation, the viscosity effects are intrinsically considered within the measurement. The main issues to tackle in an aeroacoustic problem still are:

- wide range of length scales that must be considered because of the difference between the fluid dynamic and the acoustic scales,
- nonlinearities in the governing equations,
- high Reynolds and Mach numbers.

The technique proposed can be a valuable support to approach those issues.

3 Experimental setup

The noise produced by an ideal jet in the absence of shock waves is due to the turbulence generated by the mixing of the high-pressure flow and the surrounding fluid, at ambient conditions. In this work the jet produced by a nozzle with exit diameter of 0.011 m and conicity of 6.6° has been studied (see Fig. 3). The nozzle was mounted downstream of a pipe 0.5 m long and of 0.019 m diameter. The pressure ratio measured on the nozzle was 1.205 ($M = 0.52$), and the mean exit velocity of the flow was 179.5 m/s. The corresponding Reynolds number was 132×10^3. The
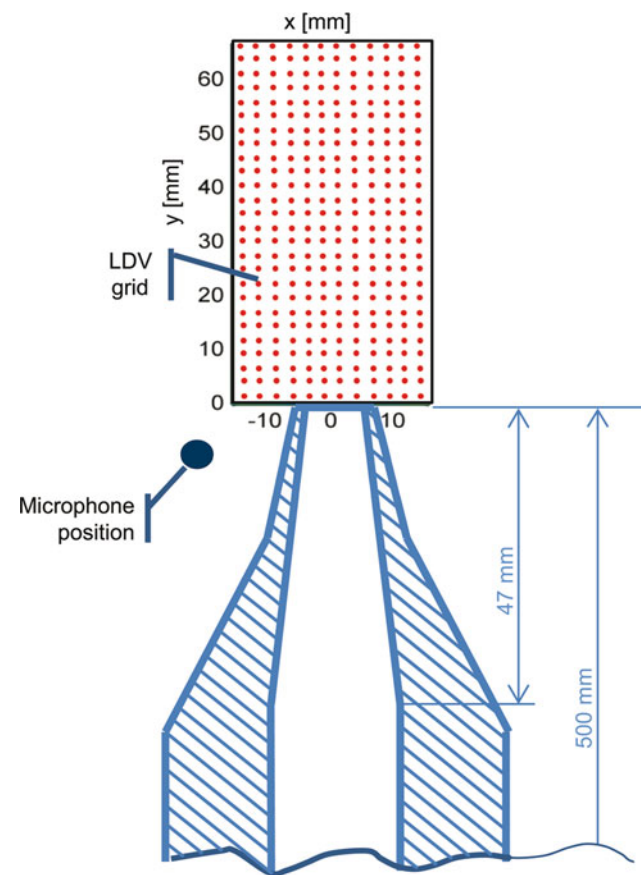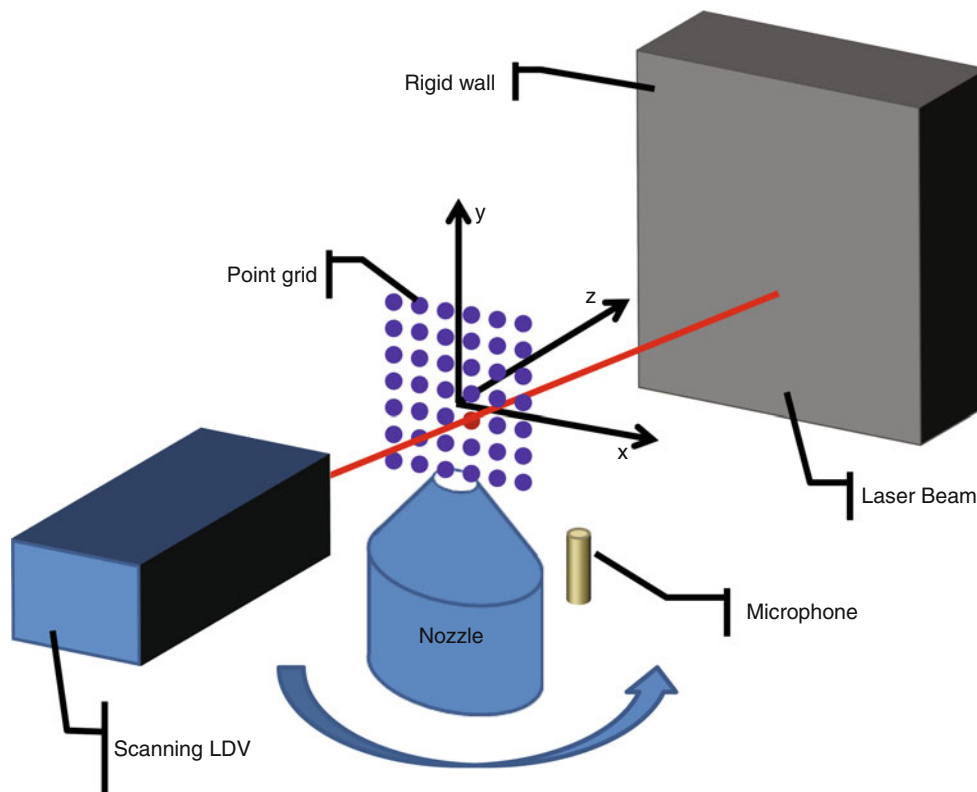

Fig. 3 Nozzle sketch and visualization of the LDV measurement positions (in *red*) and of the microphone location (*black dot*)

Fig. 4 TLI experimental setup

aeroacoustic spectral components of the flow downstream the nozzle belong mainly to two families:

- cavity resonances of the pipe, spaced of about 268.5 Hz, it being the fundamental acoustic cavity frequency,
- vortex street frequency and its high-order harmonics.

The vortex street frequency occurs because downstream the nozzle lips there is the detachment of annular von Karman vortexes that, under certain pressure and velocity conditions, produce an audible whistle. The vortex street frequency (f_v) can be calculated from the aerodynamic velocity of the flow (u), its Strouhal number (N_{st}), and the nozzle diameter (D):

$$f_v = \frac{N_{st} u}{D} \tag{11}$$

Considering a pressure ratio of 1.205, mean flow velocity of 179.5 m/s, and Strouhal number of 0.18 (for Reynolds number between 2×10^4 and 2×10^5), the vortex street frequency is about 2,937 Hz. The TLI test has been conducted using a Polytec PSV200 Scanning LDV, which measures the density fluctuation across the flow, and a B&K microphone type 4593 placed in the near field slightly downward the jet exits in order for it not to be invested by the flow, used as reference. The measurement setup is shown in Fig. 4. The acquisition

parameters were the following: 20 kHz of frequency bandwidth, 80 ms of acquisition time, and 32 averages measured at each LDV position, aiming at producing a statistically valid set of pseudo-velocities. The number of measurement points located on a 2D grid, sketched in Fig. 3, was 1,593. The flow field was measured from 360 points of view of the LDV, e.g., 360 projections obtained by rotating the nozzle with an angular resolution of 0.5° (see Fig. 4).

4 Analysis of results

The raw signals measured by LDV are pseudo-velocities related to the optical path variation because of the density fluctuation. These data, processed in frequency domain, have been averaged over the complete set of measurement positions to give the averaged spectrum shown in Fig. 5, bottom plot. In the top plot of that figure, the reference microphone spectrum is also reported. In both the spectra, two phenomena occurring at different frequencies are noteworthy. The first and most evident is the one arising at 2,937 Hz, which is the nozzle vortex street frequency (f_v). Very sharp peaks occur at higher harmonics of f_v which are originated by the acoustic excitation, which is the second phenomenon. Such phenomenon is due to the cavity resonances of the pipe placed upstream the nozzle. Those frequencies start from 268.5 Hz and continue up to the high-

order harmonics (up to at least 8 kHz). The pseudo-velocity distributions at three different frequencies (the vortex street frequency, its third harmonic, and the pipe cavity resonance at 4,837.5 Hz) are shown in Fig. 6. Those maps are the pseudo-velocity instant value spatial distributions. The instant value is a compact way of illustrating a complex vector in terms of both its amplitude and phase. Being ($|FFT_{p-v}|$) and ($\angle FFT_{p-v}$) the amplitude and phase of the pseudo-velocity signal (FFT_{p-v}), its instant value is given by the following relationship:

$$FFT_{p-v} = |FFT_{p-v}| \cos \angle FFT_{p-v} \tag{12}$$

The pseudo-velocity distributions illustrated in Fig. 6 present large-scale ordered structures representing the turbulence, the so-called wave packets, typically due to the integral of the annular vortexes appearing at the nozzle exit. Their spatial separation is of about 25 mm corresponding to the ratio of the vortex speed and its frequency (f_v). The structured turbulence is the source of the pressure fluctuation which produces the sound called "bird tone" (Goldstein 1976). This phenomenon was observed by Schram et al. (2002) from the fluid-dynamic point of view, by using PIV. In the pseudo-velocity distribution at frequency 8,837.5 Hz, a second phenomenon is evident, that

is, the acoustic wave propagation effect. Such effect is the typical propagation from spherical sources where the source is the jet core. At frequencies lower than 8,837.5 Hz, the region observed by the TLI is too limited and the spherical propagation not captured. By applying Eqs. (9) and (10), density and pressure oscillations can be estimated from the pseudo-velocity. The 3D pressure distributions obtained after tomographic reconstruction at the three frequencies considered above are reported in Figs. 7, 8, and 9 in terms of their instant value (left plot) and amplitude (right plot). Such distributions have been cut at their central section in order to make the pressure fluctuations in the jet core visible. At the vortex street frequency, the one where the noise is mostly concentrated, the sound pressure (Fig. 8) reaches the maximum value of about 300 Pa (i.e., 140 dB) in the jet core region, extended up to 5 diameter of the jet. In the highest-frequency plots (Figs. 8, 9), the core region extension decreases up to 1–1.5 diameters. At the vortex street frequency third harmonic (8,837.5 Hz, Fig. 9), the far-field propagation is visible as yellow x–z planes located along the y-axis.

5 Acoustic properties of the flow

The TLI technique is a valid experimental method for the characterization of the noise generated by a jet, although such characterization remains a difficult task, the development of the turbulent flow being a highly complex phenomenon. However, thanks to the high-frequency bandwidth of laser interferometry, such technique is able to identify the main flow properties. In this paragraph, jet aeroacoustics will be studied at different frequency ranges in order to separate phenomena occurring at low and high frequencies. First, the overall pseudo-velocity and sound pressure generated by the jet under test are presented in Figs. 10 and 11, respectively, where both the quantities are given in terms of rms on the entire measured frequency range (e.g., 10 ± 9.5 kHz). Both the 3D spatial distribution
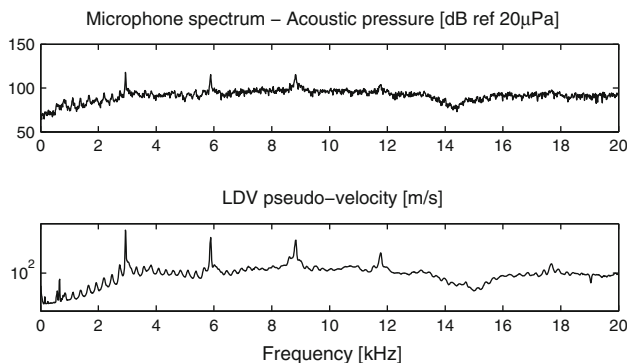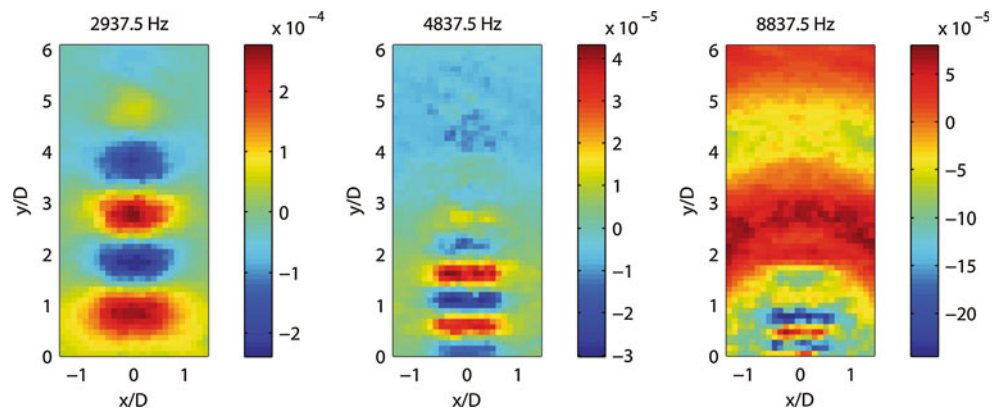
Fig. 5 Acoustic pressure (top) and TLI pseudo-velocity (bottom) spectra

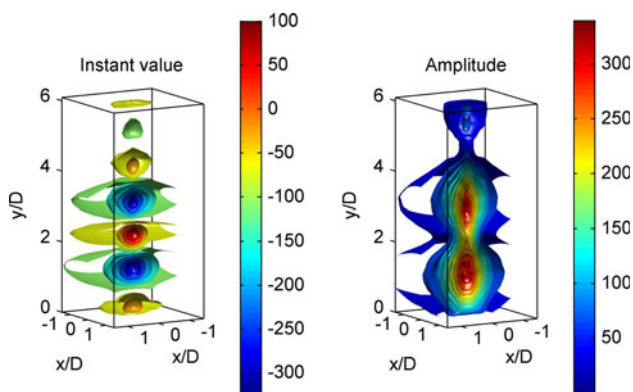Fig. 6 Pseudo-velocity instant value distributions in m/s (±12.5 Hz rms values)

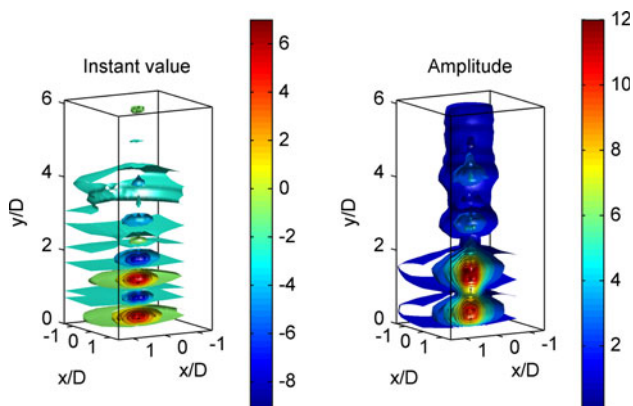**Fig. 7** Overall pressure distribution (Pa) at the vortex street frequency (2,937.5 ± 12.5 Hz rms values)

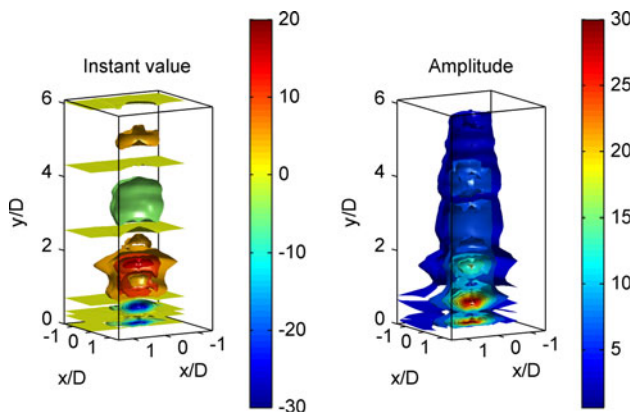**Fig. 8** Overall pressure distribution (Pa) at the pipe cavity resonance (4,837.5 ± 12.5 Hz rms values)

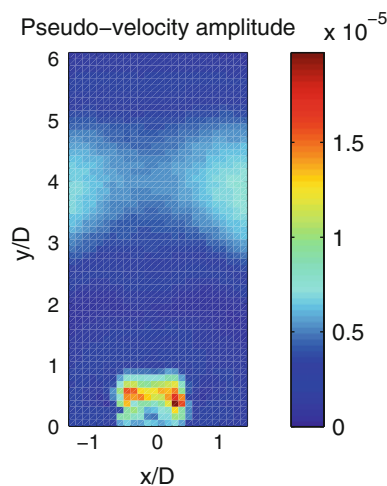**Fig. 9** Overall pressure distribution (Pa) at the third harmonic of the vortex street frequency (8,837.5 ± 12.5 Hz rms values)

Fig. 10 Overall pseudo-velocity amplitude in m/s (rms @ 10 ± 9.5 kHz)

high-frequency contents of the jet flow have been analyzed. In the low frequency range (rms @ 4.8 ± 1 kHz), the pseudo-velocity measured by TLI shows that the main region of refraction index fluctuation is located within the jet core (Fig. 12) and the far-field propagation is not visible. The sound pressure rms given in Fig. 13 in terms of 3D spatial distribution (Fig. 13, left) and central line profile (Fig. 13, right) evidences the vortex structures located in the jet core. In Fig. 14, left plot, the radial pressure fluctuation is reported at several distances from the nozzle, which are indicated in the central line profile (Fig. 13, right). The radial pressure fluctuation normalized with respect to the central line pressure (Fig. 14, right) shows the alignment of the sound pressure at the different distances and evidences the separation of the vortexes, due to their annular structure. The noise radiated at the high frequency range is characterized by high-pressure oscillation located in the jet core region, whose extension is smaller than 1 diameter, but in aerodynamic terms, the prominent phenomenon is the randomly developing turbulence dominating in the sideline direction. The typical V-shape is evident in the pseudo-velocity amplitude shown in Fig. 15, and in the sound pressure instant value, although partially masked by the far-field propagation (Fig. 16). The sidelobes centered around the jet core, visible in the radial pressure fluctuation normalized with respect to the central line pressure (Fig. 17, left plot), confirm the phenomenon of the turbulence occurring at sideline directions. The variation in directivity of the flow jet depending on the frequency range, clearly visible in Figs. 12 and 15, can be synthesized with directivity plots as the ones presented in Fig. 18, left and right plot, for the low and high frequency ranges, respectively. In agreement with the literature (Bogey et al. 2007), the maximum directivity is at around

(Fig. 11, right) and the central line profile (Fig. 11, left) evidence the coherent structures, i.e., the vortex shedding, developing in the core jet, up to 1.5 diameters, and the far-field propagation, above 1.5 diameters. Then the low- and

Fig. 11 Sound pressure instant value in Pa and central line profile (rms @ 10 ± 9.5 kHz)
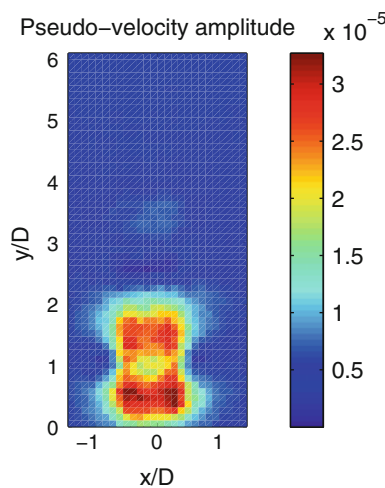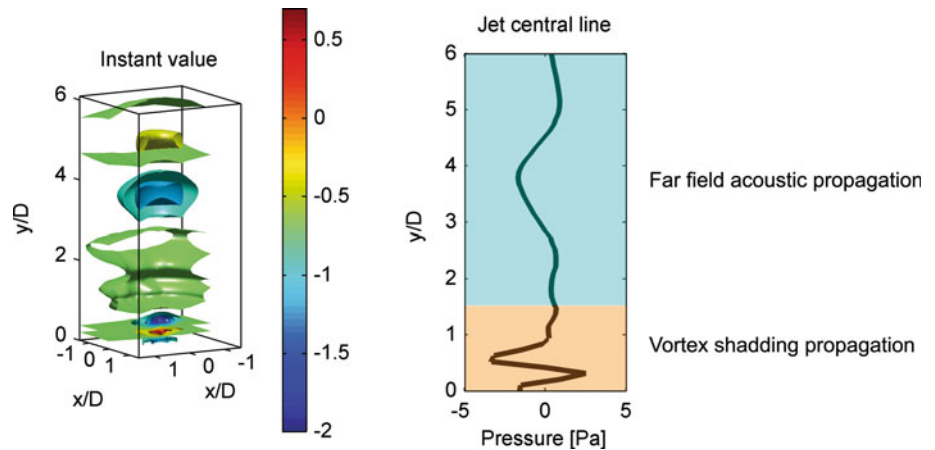

Fig. 12 Low frequency range pseudo-velocity amplitude in m/s (rms @ 4.8 ± 1 kHz)

$30°$ in the low frequency range and at $70°$ in the high frequency range.

6 Measurement uncertainty

Uncertainty assessment is an important issue in measurement procedures, mainly when they consist in an experimental phase and a significant numerical data processing. Measurement uncertainty can be estimated according to "Guide to the expression of uncertainty in measurement," (2008), when the uncertainty contribution of each input and the comprehensive mathematical model of the measurement procedure are known. On the other hand, when the procedure includes significant numerical processing, the "Guide to the expression of uncertainty in measurement," (2008), cannot be applied. In that case, the procedure result can be significantly spoiled because of convergence problems due to input data that are affected by noise. The effect of numerical processing on the procedure result cannot be easily

synthesized by a weighting function as in the case of analytical problem formulations. A very powerful technique to tackle this issue is the Monte Carlo approach (Evaluation of measurement data 2008). The TLI system includes both a mathematical model ((9) and (10)) and a computer tomography numerical process; therefore, both the contributions to the overall uncertainty must be taken into account as presented in Castellini and Martarelli (2006). The uncertainty related to the mathematical model has been evaluated by considering a type B approach following the standard (Guide to the expression of uncertainty in measurement 2008). The model input data, see (9) and (10), are the pseudo-velocity measured by the laser Doppler interferometer and the optical path. However, a further variable to be taken into account is the temperature, which influences both air density and the sound pressure. The latter, indeed, is directly related to air density by means of sound speed (c_∞):

$$c_\infty = \sqrt{\gamma R T} \tag{13}$$

That holding, sound pressure can be expressed as a function of the pseudo-velocity, optical path, and air temperature:

$$p = f(v_{\mathrm{meas}}, Z, T) \tag{14}$$

The type B uncertainty analysis allowed us to identify the most influent parameter, which is the measured pseudo-velocity (68 %). The second influencing parameter is the temperature (T) with an influence on the overall variance of 32 %. This indicates that the temperature must be kept carefully under control during the measurement process. The extended uncertainty associated with the pressure measurement is of 4.26 Pa. With 2 °C of temperature variability, the acoustic pressure uncertainty is of 1.6 dB considering a SPL of 120 dB (typical value for the jet flow). If the temperature variability increases to 10 dB, the uncertainty becomes more important, rising up to 4 dB. The uncertainty related to the CT reconstruction has been evaluated by Monte Carlo simulation, allowing us to identify the processing parameters (i.e., noise

Fig. 13 Low frequency range sound pressure instant value in Pa and central line profile (rms @ 4.8 ± 1 kHz)
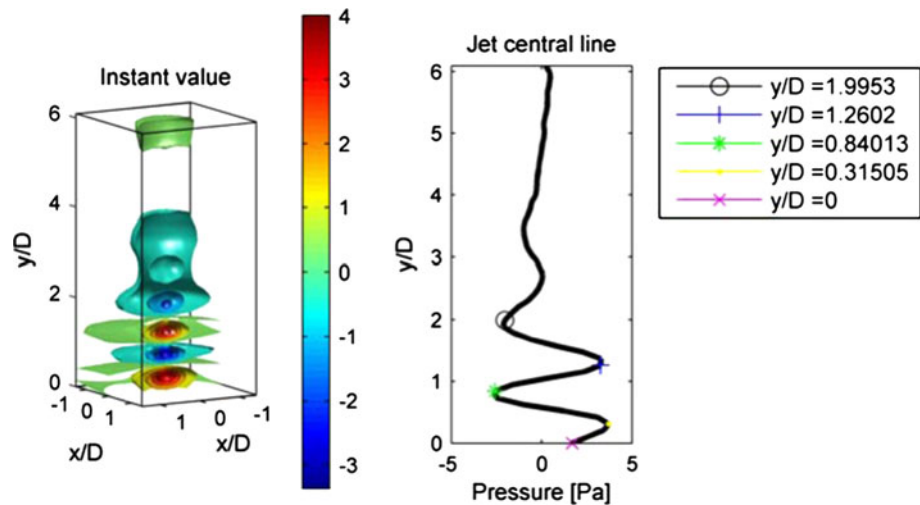

Fig. 14 Low frequency range sound pressure amplitude (*left*) and normalized amplitude with respect to the central line profile (*right*) at several distances from the nozzle (rms @ 4.8 ± 1 kHz)
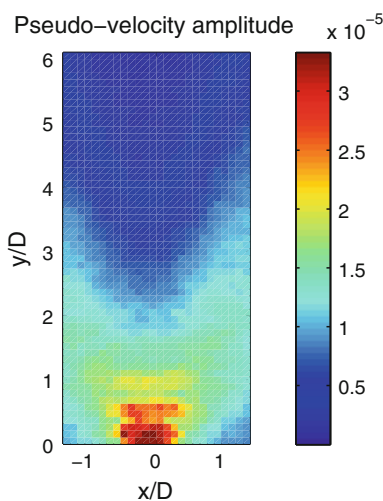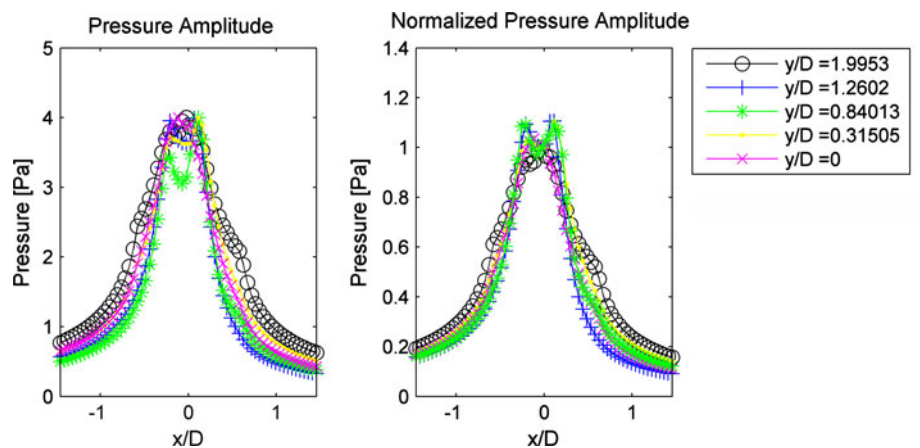

Fig. 15 High frequency range pseudo-velocity amplitude in m/s (rms @ 17.7 ± 1 kHz)

spoiling the input data, filter type and length, interpolation method, number of projections, and spatial resolution at each projection) that most influence the reconstructed data. It has been demonstrated that the most sensitive parameters are the number of projections (or angular resolution) taken in the reconstruction process and the noise spoiling the sound pressure calculated by 10. By applying the Monte Carlo simulation, the tomographic-process-averaged modulation transfer function (MTF) has been calculated, allowing us to evaluate the response of the CT algorithm in terms of spatial resolution. The averaged MTF obtained for different angular resolution (i.e., number of Radon projections) is shown in Fig. 19, which demonstrates the large sensitivity of the reconstruction to the number of projections used in the CT process. For bad angular resolution, i.e., larger than 10°, important artifacts (amplification at some spatial frequencies) appear. Angular resolution lower than 1° can be accepted for ordinary applications.

7 Aeroacoustic validation

A simple test has been designed to perform a quantitative validation of the TLI technique in terms of sound pressure obtained as the measurement output. The test

Fig. 16 High frequency range sound pressure instant value in Pa and central line profile (rms @ 17.7 ± 1 kHz)
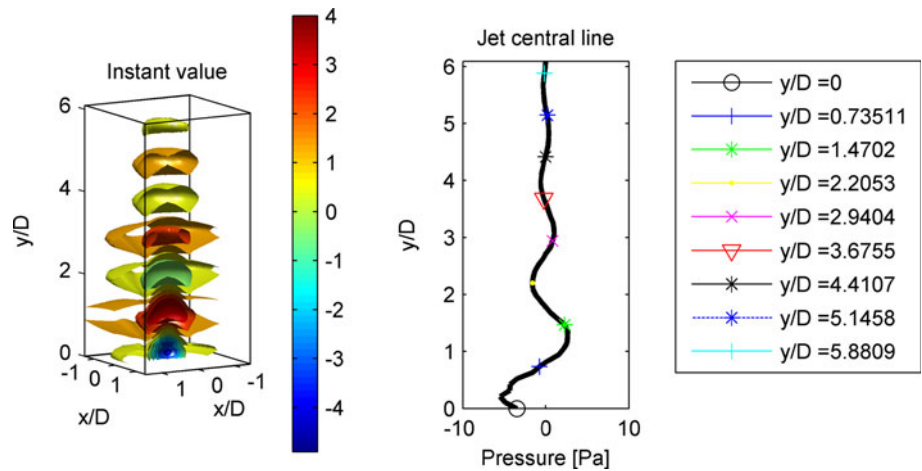

Fig. 17 High frequency range sound pressure amplitude (*left*) and normalized amplitude with respect to the central line profile (*right*) at several distances from the nozzle (rms @ 17.7 ± 1 kHz)
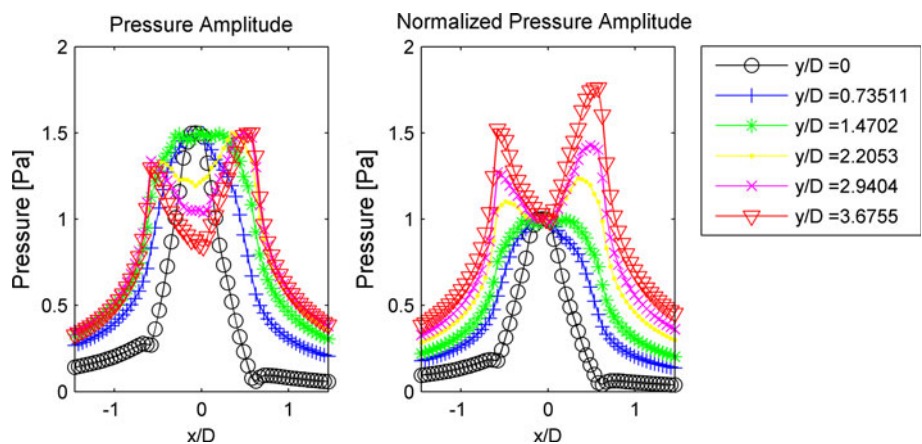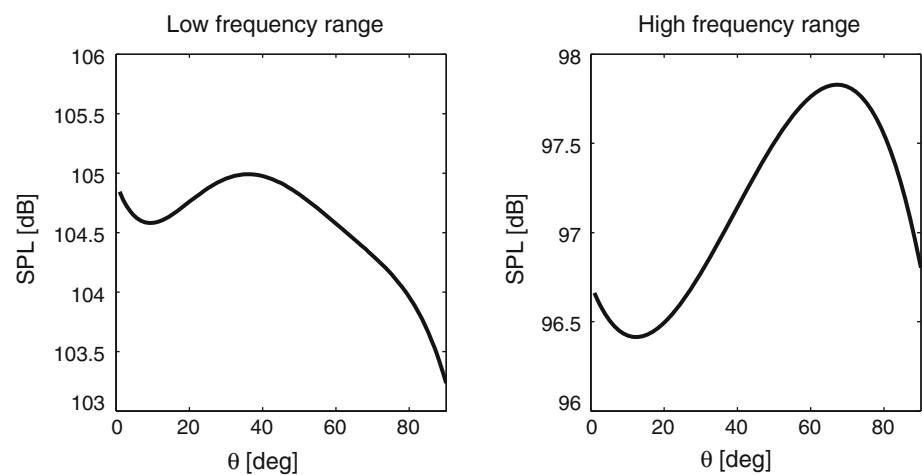

Fig. 18 Low (rms @ 17.7 ± 1 kHz) and high (rms @ 4.8 ± 1 kHz) frequency range sound pressure directivity

consisted in a loudspeaker emitting a sound field at about 4 kHz and a on-axis microphone at a distance of 0.45 m, aligned with the laser beam as shown in Fig. 20. The scanning LDV was installed in such a way that the laser beam made a line scan on a plane almost tangential to the microphone diaphragm. Therefore, once the tomographic reconstruction was performed, it was possible to evaluate, by TLI, the sound pressure in front of the

Fig. 19 Modulation transfer function (MTF) for different viewing angle resolution
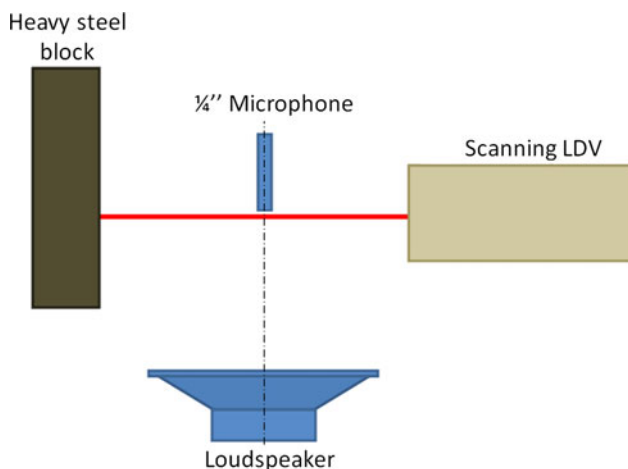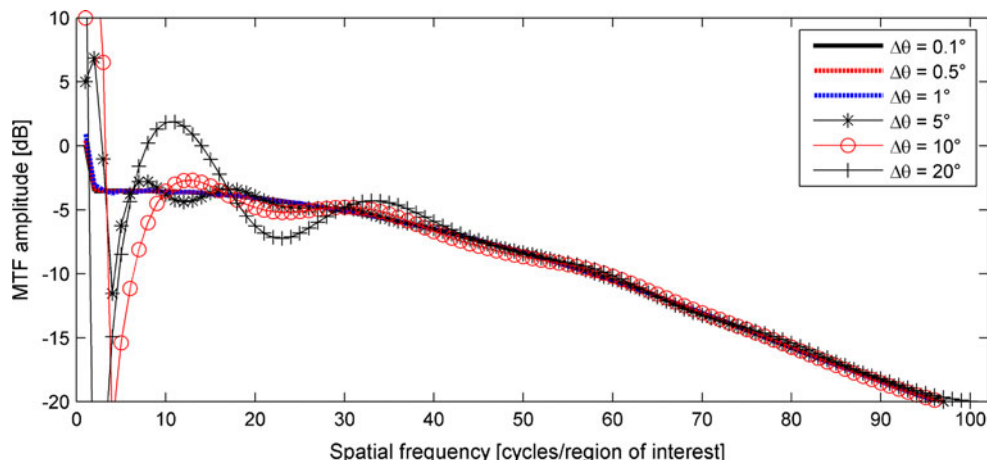

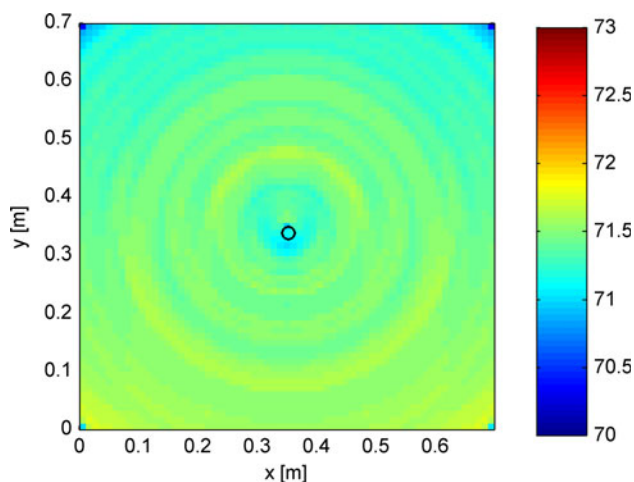**Fig. 20** Scheme of the test for aeroacoustic validation

Fig. 21 Sound pressure distribution in dB measured by TLI in front of the reference microphone

microphone and perform a quantitative comparison with a reference transducer, the microphone itself. Figure 21 shows the sound pressure reconstructed by TLI on a plane tangential to the reference microphone diaphragm, which is almost constant. The ring visible on the maps is due to CT reconstruction artifacts, but they can be considered within the measurement uncertainty (1.6 dB) as stated in the previous section. The sound pressure measured by TLI was 71.7 ± 1.6 dB, which was perfectly compatible with the one measured by the microphone (72.9 dB).

8 Conclusions

In this work an interferometric technique joined to a tomographic reconstruction algorithm has been applied for the complete aeroacoustic characterization of a subsonic jet. The procedure makes it possible to indirectly measure the air density variation within the measurement volume downstream the jet from the air refraction index and subsequently to calculate the acoustic pressure generated by the jet itself. A complete characterization of the subsonic jet aeroacoustics has been presented, the technique being able to measure the pressure fluctuation due to both aerodynamic phenomena (the cause) and acoustic ones (the effect). Concerning the analysis of the aerodynamic cause, both the low- and high-frequency contents of the sound field generated by the turbulence have been analyzed. Two-dimensional spatial distribution and directivity plots of the acoustic pressure made it possible to evidence phenomena occurring at different frequency ranges, as the coherent vortex shedding (2–6 kHz) and the randomly developing turbulences (16–18 kHz). Finally, the uncertainty related to the measurement procedure has been presented together with a simple test for a quantitative aeroacoustic validation of the technique.

References

Anderson JD (1991) Fundamentals of aerodynamics. McGraw-Hill Int. Editions, New York

Bogey C, Barré S, Fleury V, Bailly C, Juvé D (2007) Experimental study of the spectral properties of near-field and far-field jet noise. Int J Aeroacoust 6(2):73–92

Born M, Wolf E (1959) Principles of optics: electromagnetic theory of propagation, interference and diffraction of light. Cambridge University Press, Cambridge

Castellini P, Martarelli M (2006) In: Conference proceedings of the society for experimental mechanics series

Castellini P, Martarelli M (2008) Acoustic beamforming: analysis of uncertainty and metrological performances. Mech Syst Signal Process 22(3):672

Dougherty R, Podboy G (2009) In: 15th AIAA/CEAS aeroacoustics conference (30th AIAA aeroacoustics conference)

Edlén B (1966) The refractive index of air. Metrologia 2:71–80

Evaluation of measurement data—supplement 1 to the "Guide to the expression of uncertainty in measurement", ISO, Geneve (2008)

Fischer A, Sauvage E (2008) In: 14th international symposium on applications of laser techniques to fluid mechanics, Lisbon, Portugal

Giuliani F, Leitgeb T, Lang A, Woisetschläger J (2010) Mapping the density fluctuations in a pulsed air-methane flame using laser-vibrometry. ASME J Eng Gas Turbines Power 132:031603

Goldstein ME (1976) Aeroacoustics. McGraw-Hill, New York

Guide to the Expression of Uncertainty in Measurement, ISO, Geneve (2008)

Köberl S, Fontaneto F, Giuliani F, Woisetschläger J (2010) Frequency-resolved interferometric measurement of local density fluctuations for turbulent combustion analysis. Meas Sci Technol 21(3):035302

Kleine H, Gronig H, Takayama K (2006) Simultaneous shadow, Schlieren and interferometric visualization of compressible flows. Opt Lasers Eng 44:170

Lorentz HA (1880) Ueber die Beziehung zwischen der Fortpflanzungsgeschwindigkeit des Lichtes und der Korperdichte. Wied Ann Phys 9:641–665

Lorenz L (1880) Ueber die Refractionsconstante. Wied Ann Phys 11:70–103

Mayrhofer N, Woisetschläger J (2001) Frequency analysis of turbulent compressible flows by laser vibrometry. Exp Fluids 31(2):153–161

Merzkirch W (1974) Flow visualization. Academic Press, Inc, London

Radon J (1917) Uber die bestimmung von funktionen durch ihre integralwerte langs gewisser mannigfaltigkeiten. Ber Der Sachs Akad Der Wissensch 29:262

Schram C, Romera G, Hirschberg A, Riethmuller M (2002) In: Proceedings of the 2002 international conference on noise and vibration engineering, ISMA, pp 261–270

Tatar K, Olsson E, Forsberg F (2007) In: ICEM13, Alexandroupolis, Greece

Vanherzeele J, Brouns M, Castellini P, Guillaume P, Martarelli M, Ragni D, Tomasini EP, Vanlanduit S (2007) Flow characterization using a laser Doppler vibrometer. Opt Lasers Eng 45(1):19–26

Violato D, Scarano F (2011) Three-dimensional evolution of flow structures in transitional circular and chevron jets. Phys Fluids 23:124104

Woisetschläger J, Mayrhofer N, Hampel B, Lang H, Sanz W (2003) Laser-optical investigation of turbine wake flow. Exp Fluids 34(3):371–378

Zipser L, Franke H (2002) In: International conference in vibration measurements by laser techniques, Ancona